Review on Plasma Electrolytic Oxidation of Titanium Coatings

V.Srinivasan, P.Karthik, P.Mukesh, S.Praven Kumar

[1]Assistant professor, [2, 3, 4] U.G Student, Department of Mechanical Engineering

Sri Ramakrishna Engineering College, Tamilnadu, India

Abstract: The titanium coatings namely, Titanium, Nitrogen doped TiO, and Titanium oxide was analysed in terms of their electrochemical corrosion and surface properties in virtual body fluid in accordance to their on-field applications. The electrolytes such as phosphate and silicate are used in a waveform of square pattern with frequency of 50Hz. These coatings were deposited onto stainless steel substrates by plasma surface alloying technique. Morphology, composition, and structure were investigated by X-ray Diffuser and the coefficient of friction is better with the phosphate electrolyte. Corrosion resistance analysis shows that Titanium (Ti), Titanium oxide, and Nitrogen doped TiO2 coatings highly resistant to corrosion polarization and a better corrosion potential of high stability and also reduces the wear life.

Keywords: Plasma Alloying Technique, Titanium, Electrolyte

I INTRODUCTION

Introduction of Plasma electrolytic oxidation (PEO) is being studied extensively as a method of coating light alloys, especially for wear resistance, corrosion protection and biocompatibility.[1-3]. The coatings are formed by polarizing the metal to the dielectric breakdown voltage in a suitable electrolyte. A wide range of polarization conditions are available for formation of the coatings, including DC and AC, with control of the current, voltage or power supplied to the cell. Under AC conditions, a variety of waveforms and frequencies can be employed. The coatings can be formed to many microns in thick-ness and are composed of species derived from the substrate and the electrolyte in amounts dependent upon the conditions of coating formation. The coating material is generated at the sites of micro discharges on the polarized metal that give rise to very high local current densities, temperatures and pressures[4]. Solid solution austenitic phase (γ) with high chromium content (12% to 20%) is generally responsible for the excellent corrosion performance of austenitic alloys. This advantage allows the use of these alloys in biomedical, public, and food industries as well as in kitchen appliances [5-6]. Titanium and its alloys are widely used for fabrication of orthopaedic and dental implants because of their good biocompatibility, high tensile strength, fracture toughness and fatigue strength [7]. The high temperatures that are reached locally in the coating allow the formation of a variety of crystalline and amorphous phases. The crystalline phases can give rise to coatings of high hardness and wear resistance. The mechanism of coating material formation remains the subject of discussion, but it is likely to involve several processes, including anodic oxidation, thermal oxidation, thermolysis, and reactions of substrate and electrolyte species within the plasmas generated by the discharges. In the case of titanium and titanium alloys, PEO coatings have been of particular interest for improvement of the tribological behaviour and of the biocompatibility of the substrates. A wide variety of forming conditions have been investigated, producing films of differing compositions, morphologies and thicknesses. Shokou-far et al. formed coatings of a few microns thickness on titanium using pulsed DC at 350 V, a frequency of 1000 Hz, a duty cycle of 40% and a treatment time of 3 min [8]. Various surface modification technologies, such as nitriding, carburizing, nitro carburizing, physical vapour deposition, and chemical vapour deposition, among others, have been used to improve the corrosion properties of austenitic SS. However, the poor durability of traditional thin-surface layers has limited their use in common medical applications. The decrease in corrosion resistance is caused by the heavy precipitation of chromium carbide and chromium nitride on grain boundaries, which are surrounded by chromium-depleted zones [9-10]. A several algorithms were developed for the estimation of fractal dimension from atomic force microscopy (AFM) images, but the most commonly Fourier-spectra (power spectrum)were used. The reliability of this method was tested with regard to

the difference between estimated and simulated fractal dimension as error measure. Simulated fractal dimension was computer generated fractal surface images with known fractal dimension. A similar approach was applied to study the influence of tip of geometry on the fractal dimension estimated from AFM images [11]. This research is triggered by the fact that the band gap of WO3 is 2.4–2.8 eV and both the upper edge of the valence band and the lower edge of the conduction band of WO3 are lower than those of TiO2. Thus, WO3 can be excited by illumination with visible light. Bi-component WO3 and TiO2 materials have shown enhanced photocatalytic activity with respect to their plain component analogs, since their valence and conduction band energy diagrams favor electron injection from the conduction band of TiO2 to that of WO3 and hole transfer between valence bands in the opposite direction. This, in turn, reduces electron hole recombination in both semiconductors [12]. Porous structures in anodic coatings are potentially favourable for the addition of material that improves the surface properties, for example a solid lubricant material, such as polytetra- fluoro ethylene (ptfe), or a secondary coating. For example, Zou et al. incorporated fluoro polymer particles into a porous alumina film by either hot-dipping or electrophoretic deposition. Liu et al. synthesized hard anodic coatings containing ptfe particles on AA 6063aluminium alloy by adding the particles to the electrolyte. Kuang et al. showed that combinations of metal oxide particles and ptfe can provide both high micro hardness and good self-lubricating properties. Various particles, such as oxides, clay and ptfe, have been incorporated into PEO coatings on aluminium and magnesium to improve the properties of the coatings. Rudnevet al. incorporated ptfe into PEO coatings formed on an aluminium alloy under galvano static conditions. The silicate-based electrolyte contained dispersed solid ptfe and siloxane–acrylate emulsion. High loadings of ptfe resulted in the contact angle between the coating and water droplets being similar to that using bulk ptfe. A relatively high ratio of carbon to fluorine in the coating suggested that the ptfe was partially degraded during PEO. A similar approach was used to form coatings that contained graphite particles on a titanium alloy [13-16]. The aim of this work is to obtain further insight into surface morphology by means of fractal geometry of the surface as a contemporary approach to the surface analysis. Within present study the surface fractal dimension of the TiO2/WO3 coatings was evaluated using high resolution AFM imaging, in order to test its sensitivity with respect to the change of surface morphology as the consequence of PEO process duration. Wei et al. [17] fabricated TiO2-based coating containing amorphous Ca and P compounds on Ti6Al4V by PEO technique. The results indicated that the TiO2coating containing low crystallinity and amorphous calcium phosphate could facilitate the formation of apatite. From the open literature many works suggested that the formation of Ca and P compounds have a beneficial effect on the bioactivity of the TiO2layers. Based on these facts, fabricating a Ca and P incorporated TiO2coating by PEO treatment should further improve the bioactivity of NiTi alloy. However, considering the high content of Ni in NiTi alloys, the PEO treatment applied on NiTi alloys is not as easy as on Ti and the other Ti alloys because Ni is a kind of non-valve metal. How to fabricate desired elements incorporated PEO coating, especially TiO2coating on NiTi alloy, is still a challenge. Therefore, the present work will use a new kind of organic electrolyte which selected ethylene glycol as solvent, and TiO2col-losol (Ti-sol) and calcium glycerol phosphate (Ca-Gp) as additive for the PEO processing of NiTi, aiming at forming a Ca, P incorporatedTiO2coating. The coating will be characterized in terms of surface morphology, phase construction, chemical composition, corrosion resistance, and bonding strength. The apatite-forming ability of the obtained coating will be also evaluated in a simulated body fluid (SBF).

II MATERIALS AND METHODS

A.MATERIALS:

AISI 316L stainless steel discs of 20 mm in diameter and 5 mm in thickness with mirror surface finish (Ra<0.1 μm) were used as the coatings substrates. Ti and TiN coatings were prepared on SS substrates by plasma surface alloying technique. The sputtering target was Ti of 99.9% purity. The chamber was evacuated down to 1 Pa and flushed with pure argon several times prior to sputtering. The SS specimens were cleaned by argon ion bombardment prior to surface alloying. Argon gas and Ar-N2 mixture gas were controlled using mass flow controllers. The following parameters were selected for both Ti and TiN coatings: the chamber pressure was kept at 40 Pa, the distance between the sputtering target and substrate sample was 15 mm, the substrate temperature was at 900℃, and the processing time was 2 h. For Ti coatings, the target voltage was controlled at -1100 to -1150 V and the substrate voltage at -500 to -550 V. For TiN coatings, the target voltage was controlled at -1000 to -1050 V, the substrate voltage was at -450 to -500 V, and the flux mixing ratio of Ar/N2 was 1/2. The TiO2 and

N–TiO2 coatings were prepared by oxidative annealing the resulted Ti and TiN coatings in air, respectively. Both the Ti and TiN coatings were subsequently annealed in air at 450 ◦C for 2 h to oxidize and crystallize the samples. Conditions Commercial purity 99.6% titanium sheet, of 1.0 mm thickness was obtained from ADVENT Research Materials Ltd., England. The composition of the titanium according to optical emission spectroscopy (OES), which analysed the metallic constituents of the titanium, is given in Table 1. Rectangular specimens were cut from the sheet and ground to a 1200 SiC grade finish. They were then degreased with acetone, washed with distilled water dried in air at 40 ◦C and, finally, coated in lacquer (Stopper 45MacDermid), leaving working areas of ∼1.0 cm2. AC PEO treatment was carried out at a constant rms current density with a square waveform, employing different negative to positive (peak-to-peak) current ratios (in/ip), using an ACS-FB power supply (ET systems electronic GmbH). The frequency was 50 Hz, with a duty cycle in the range 30–70%. An aqueous electrolyte was prepared by dissolving reagent grade sodium silicate (10.5 g l−1specificgravity 1.5), phosphoric acid (2 ml l−1) and potassium hydroxide (2.8 g l−1) in deionized water. The conductivity and pH of the electrolyte were 10.2 mS cm−1and 12.2 respectively. The electrolyte, of volume 1 dm−3, was stirred with a magnetic stirrer during PEO. A double-walled glass cell was employed to contain the electrolyte. The temperature of the electrolyte was kept at25 ◦C by a flow of cold water through the cell wall. A stainless steel (type 304) plate of dimensions 7.5 × 15 cm was used as a counter electrode. The applied current density was in the range200–900 mA cm−2(rms), with treatment times of up to 3600 s. Voltage (rms)–time responses were recorded electronically during anodizing, employing Lab-View software with a sampling time of 20 ms. The data acquisition system for monitoring of the volt-age employed National Instruments (NI) SCXI high-performance signal conditioning and switching platforms. The set-up included two isolation modules with terminal blocks installed in the SCXI-1000 chassis. The first module had a NI TBX-1316 terminal block connected to it. The second one had an SCXI-1328 terminal block. Light emission of the discharges was collected using an optical emission spectroscope (USB4000 Ocean Optics), with an optical fibre immersed in the electrolyte, and located a few centimetres from the specimen to optimize the collected light intensity and to reduce absorption from the bath. The polarisation-resistant optical fibre (ZFQ-9596, Ocean Optics), with PVDF sleeving and a PEEK ferrule, was of 1000m diameter, with a numerical aperture of0.22 ± 0.22. Emission spectra were recorded in the wavelength range 200–850 nm with a spectra resolution of 1 nm.

B. METHODS:

I SEM/EDS Method of Evaluation:

The adhesion between titanium and dental porcelain is related to the diffusion of oxygen to the reaction layer formed on cast-titanium surfaces during porcelain firing. The diffusion of oxygen could be suppressed by coating the titanium surface with a thin gold layer. This study characterized the effects of gold coating on titanium-ceramic adhesion. ASTM grade II CP titanium was cast into a MgO-based investment (Selevest CB, Selec). The specimen surfaces were air abraded with 110-microm Al(2)O(3) particles. Gold coating was applied on titanium surfaces by three methods: gold-paste (Deck Gold NF, Degussa-Ney) coating and firing at 800 degrees C for three times, single gold-paste coating and firing followed by sputter coating (40 mA, 500 s), and sputter coating (40 mA, 1000 s). Surfaces only air abraded with Al(2)O(3) particles were used as controls. An ultra-low-fusing dental porcelain (Vita Titankeramik, Vident) was fused on titanium surfaces. Specimen surfaces were characterized by SEM/EDS and XRD. The titanium-ceramic adhesion was evaluated by a biaxial flexure test (N = 8), and area fraction of adherent porcelain (AFAP) was determined by EDS. Numerical results were statistically analyzed by one-way ANOVA and the Student-Newman-Keuls test at alpha = 0.05. SEM fractography showed a substantial amount of porcelains remaining on the gold-sputter-coated titanium surfaces. A new Au(2)Ti phase was found on gold-coated titanium surface after the firing. Significantly higher ($p < .05$) AFAP values were determined for the gold-sputter-coated specimens compared to the others. No significant differences were found among the other groups and the control. Results suggested that gold coatings used in this study are not effective barriers to completely protect titanium from oxidation during the porcelain firing, and porcelain adherence to cast titanium can be improved by gold-sputter coating used in the present study.

II X-RAY DIFFRACTION:

X-ray diffraction measurements on titanium nitride coatings prepared by the physical vapour deposition method in a magnetron were performed. The peak positions, intensities, integral breadths and shape parameters have been determined and related to layer characteristics (lattice parameters, texture, strain and domain size) for several sets of samples deposited under various conditions and also with different film thicknesses. In addition, the stress was measured by the X-ray method. A strong dependence of the lattice parameters and X-ray line broadening on the crystallographic direction as well as on the line asymmetry appeared systematically for certain deposition conditions. Interpretation of this effect is not clear and therefore detailed results are presented together with some possible reasons for such an anisotropy.

III RESULTS AND DISCUSSION

A. Optical emission spectroscopy:

Optical emission spectra recorded at intervals of 60 s during PEO for 900 s at a current density of 500 mA cm with a duty cycle of 50% and an in/ip ratio of 1. Emissions were detected initially from mainly titanium (Ti I 307.8 nm), hydrogen (H _656.3 nm, H _486.1 nm, sodium (Na I 589.6 nm) and silicon (SiI 288.1 nm) species derived from the titanium substrate and the electrolyte. Small peaks were also present due to potassium (K I766.5 and 769.9 nm) and oxygen I (777.1 nm), originating from the electrolyte. Fig. 3(b) and (c) shows that the peaks for titanium, silicon and hydrogen species reduced in height with time. The voltage–time response in the inset of Fig. 3(b) was recorded during the measurements. A particularly large reduction of the titanium peak occurred after ~300 s, which is close to the shallow trough in the voltage response, when the sparks also changed in colour with the development of an orange hue. In contrast, the peaks for sodium and potassium increased by a factor of ~2.5 during the first540 s, when the maximum emission intensities were reached.

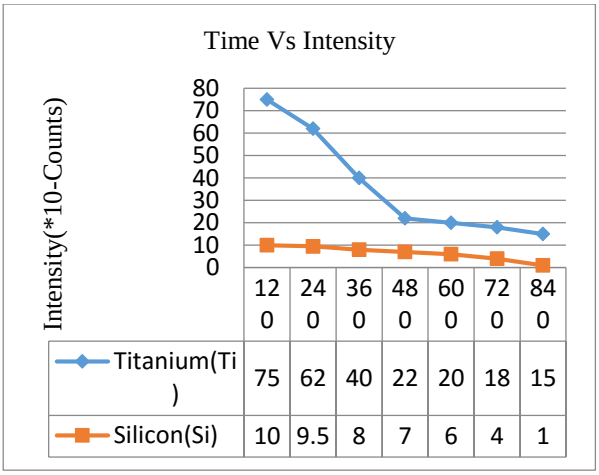

Fig 1: Optical emission spectra recorded during PEO of titanium for 900 s at 500 mA cm−2in alkaline silicate/phosphate electrolyte, with a frequency of 50 Hz, a duty cycle of 50% and a negative-to-positive current ratio of 1. (b and c) Dependence of intensity of optical emission on time of PEO treatment for emissions from titanium, silicon hydrogen, potassium and sodium species.

B. Kinetics of coating formation:

The dependence of the coating thickness on the time of PEO at500 mA cm−2, with a duty cycle of 50% and an in/ip ratio of 1 is shown in Fig. 4, using thicknesses measured by the eddy current meter and by SEM of coating cross-sections. The thicknesses were determined by the eddy current method only for those specimens that were covered uniformly by the white coating material, which occurred at times from 700 s. The measurements by SEM apply also to the white coating that formed locally at earlier times. Both methods of measurement indicated a thickness of ~30 m after 900 s, corresponding to an average growth rate of ~33 nm s−1. Thereafter, the growth rate slows, with the thickness after 1800 s reaching between 40 and 50 m. The eddy current method indicated a greater thickness at relatively long treatment times than SEM, which is probably due to the coating roughness that is shown in later scanning electron micrographs. The eddy current method also samples a relatively large area of the specimen surface contrasting with the localized measurements obtained from the cross-sections observed by SEM. Since the rate of coating growth was negligible after ~1800 s, further studies were confined to treatment times of either 900 or 1200 s. Other work has reported a similar declining rate of coating growth on a Ti–6Al–4V alloy in a silicate-hexameta phosphate electrolyte, with the rate of thickening at long times of treatment becoming very low, similar to the present observation; the slow growth correlated with the initial micro discharges

being replaced by arcs and with increase of the coating roughness

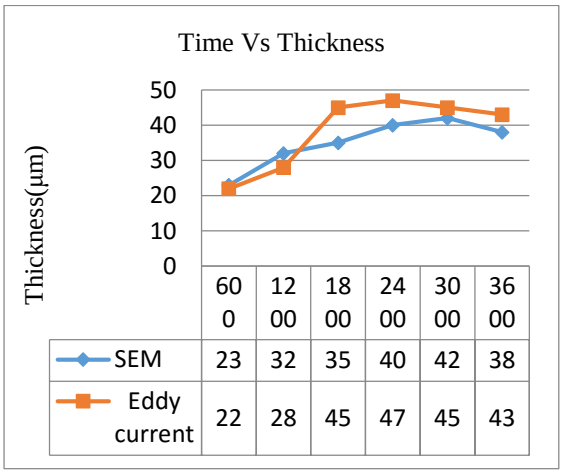

Fig 2: Dependence of the thickness of the coating on the time during PEO of titanium for 3600 s at 500 mA cm−2in alkaline silicate/phosphate electrolyte

IV CONCLUSION

PEO coatings formed at 500 mA cm−2(rms) in the alkaline silicate phosphate electrolyte, with a frequency of 50 Hz, a duty cycle of 50% and a negative-to-positive current ratio of 1, are composed of amorphous silica, anatase, rutile and Ti2O5. Phosphorus species and minor amounts of potassium and sodium species were also incorporated into the coating. The coatings are limited in thickness to ∼40 to 50m and are highly porous, with a relatively thick, silica-rich outer region and a thinner, titanium rich inner region. The silica is also present in veins that penetrate the inner, titania-rich material. The limitation of thickness is related to a relatively steep drop in the voltage after ∼900 s of PEO, with a reduction in the intensity of sparking. Similar morphologies of coatings are generated at duty cycles of 50–70% and with negative-to-positive current ratios of up to1.13, with thinner coatings being formed at reduced duty cycles and at increased current ratios. The reductions in coating thick-ness are associated with declines of the voltage and termination of sparking at relatively early stages of PEO. The coated samples would have a lower corrosion and metallic ion releasing rate. N–TiO2 coatings exhibited the best corrosion resistance for the coatings investigated in this study. This finding may be attributed to the multi layered structure (an outer oxidative layer and an inner diffusion zone of Ti and N) of N–TiO2, which can hinder the diffusion of reactive ions.

V REFERENCE

[1] P. Bala Srinivasan, C. Blawert, W. Dietzel, Effect of plasma electrolytic oxidation treatment on the corrosion and stress corrosion cracking behaviour of AM50magnesium alloy, Mater. Sci. Eng. A 494 (2008) 401–406.

[2] F. Monfort, A. Berkani, E. Matykina, P. Skeldon, G.E. Thompson, H. Habazaki,K. Shimizu, Development of anodic coatings on aluminium under sparking conditions in silicate electrolyte, Corros. Sci. 48 (2007) 672–693.

[3] J.A. Curran, H. Kalkanci, Y. Magurova, T.W. Clyne, Mullite-rich plasma electrolytic oxide coatings for thermal barrier protection applications, Surf. Coat Technol. 201 (2007) 8683–8687.

[4]. C.S. Dunleavy, J.A. Curran, T.W. Clyne, Time dependent statistics of plasma dis-charge parameters during bulk AC plasma electrolytic oxidation of aluminium Appl. Surf. Sci. 268 (2013) 397–409.

[5] I.T. Hong, C.H. Koo, Antibacterial properties, corrosion resistance and mechanical properties of Cu-modified SUS 304 stainless steel, Mater. Sci. Eng. A 393 (2005) 213-222.

[6] J. Macák, P. Sajdl, P. Kučera, R. Novotný, J. Vošta, In situ electrochemical impedance and noise measurements of corroding stainless steel in high temperature water, Electro Act a 51 (2006) 3566-3577.

[7]. M. Niinomi, Mater. Trans. 10 (2008) 2170–2178.

[8] M. Shokoufar, C. Dehghanian, A. Baradaran, Preparation of ceramic coat-ing on Ti substrate by plasma electrolytic oxidation in different electrolyte and evaluation of its corrosion resistance, Appl. Surf. Sci. 257 (2011)2617–2624.

[9] A.J. Perry, R.R. Manory, L.P. Ward, P.P. Kavuri, The effects of metal ion post-implantation on the near surface properties of TiN deposited by CVD, Surf. Coat. Technol. 133-134 (2000) 203-207.

[10] A. Tekin, J.W. Martin, B.A. Senior, Grain boundary sensitization and desensitization during the ageing of 316L(N) austenitic stainless steels, J. Mater. Sci. 26 (1991) 2458-2466.

[11] A. Mannelquist, N. Almqvist, S. Fredriksson, Appl. Phys. A 66 (1998) S891.

[12] M. Miyauchi, A. Nakajima, T. Watanabe, K. Hashimoto, Chemistry of Materials 14 (2002) 4714.

[13] H.Q. Zou, A.M. Liu, H.C. Wu, G.H. Li, C.Y. Zhang, Synergistic fluoro polymer coatings on

aluminum and its alloys, Mater. Protect. 35 (2002) 9–13.

[14] S.Y. Liu, H.C. Zhang, X.M. Gao, W. Liu, Y.Q. Shi, Study of composite hard anodizing of aluminium alloy 6063 and its friction behaviours Light Alloy Fabricat. Technol.32 (2004) 42–45.

[15] Y.F. Kuang, Y. Xu, G.X. Li, Research advances on the surface treatment of aluminium and its alloy, Plat. Finish. 22 (2000) 16–21.

[16] E. Matykina, R. Arrabal, F. Monfort, P. Skeldon, G.E. Thompson, Incorporation of zirconia into coatings formed by DC plasma electrolytic oxidation of aluminium in nanoparticle suspensions, Appl. Surf. Sci. 255 (2008) 2830–2839.

[17] D.Q. Wei, Y. Zhou, D.C. Jia, Y.M. Wang, Surf. Coat. Technol. 201 (2007)8723–8729